

Impact of Cattaneo-Christov Heat Flux in the Nanofluid Flow over an Inclined Permeable Surface with Irreversibility Analysis

Muhammad Ramzan*, Hina Gul

Department of Computer Science, Bahria University, Islamabad, Pakistan

Email: *mramzan@bahria.edu.pk

How to cite this paper: Ramzan, M. and Gul, H. (2024) Impact of Cattaneo-Christov Heat Flux in the Nanofluid Flow over an Inclined Permeable Surface with Irreversibility Analysis. *Journal of Applied Mathematics and Physics*, 12, 1582-1595.
<https://doi.org/10.4236/jamp.2024.124097>

Received: March 24, 2024

Accepted: April 27, 2024

Published: April 30, 2024

Abstract

This study discusses the magnetohydrodynamic nanofluid flow over an inclined permeable surface influenced by mixed convection, and Cattaneo-Christov heat flux. The heat transfer analysis is performed in the presence of a heat source/sink and thermal stratification. To gauge the energy loss during the process, an irreversibility analysis is also performed. A numerical solution to the envisaged problem is obtained using the `bvp4c` package of MATLAB. Graphs are drawn to assess the consequences of the arising parameters against the associated profiles. The results show that an augmentation in the magnetic field and nanomaterial volume fraction results in an enhancement in the temperature profile. A strong magnetic field can significantly reduce the fluid velocity. The behavior of the Skin friction coefficient against the different estimates of emerging parameters is discussed.

Keywords

Nanofluid Flow, Cattaneo-Christov Heat Flux, Permeable Surface, Mixed Convection, Heat Source/Sink, Thermal Stratification

1. Introduction

Carbon nanotubes (CNTs) exhibit cylindrical structures composed of carbon atoms arranged in nature-like configurations, forming thin and elongated pure carbon structures. Their diameters typically range from 1 to 50 nm. When incorporated into certain polymer compounds, CNTs enhance their damping properties and mechanical characteristics. Broadly categorized as single-wall and multi-wall CNTs, they serve both structural and non-structural purposes. Structural applications encompass thermal stability, inter-laminar shear strength, fracture

toughness, stiffness, energy absorption, strength, and damping, whereas non-structural applications involve improved thermal conductivity, energy storage, strain sensing, electromagnetic interference mitigation, and so forth. Wang *et al.* [1] experimentally examined the pressure drop and heat transmission of nanofluid flow containing CNTs in a circular tube lying in a horizontal position. Their findings revealed a notable increase in heat transfer efficiency for high values of Reynolds number. A kerosene-aqueous-based nanofluid flow with CNTs as nanoparticles over an extended surface influenced by an induced magnetic field in the presence of gyrotactic microorganisms is examined by Iqbal *et al.* [2]. An interesting result disclosed that nanoparticles' volume fraction improves the strength of the assumed magnetic field. Alharbi *et al.* [3] performed a comparative analysis of simple nanofluid and hybrid nanofluid flows with CNTs (both single-wall and multi-wall) and ethylene glycol as a base fluid over a two-directional surface with prescribed heat flux and prescribed surface temperature amalgamated with modified Fourier heat flux. It is revealed here that prescribed heat flux and prescribed surface temperature are the main sources for the rise in the temperature of the fluid. The heat transfer analysis of the nanolayer over an aqueous-based nanofluid flow comprising CNTs over a movable wedge is examined numerically by Gul *et al.* [4]. The model is supported by the convective and the slip conditions at the surface of the wedge. It is witnessed here that fluid velocity is on the decline for slip conditions. Bashir *et al.* [5] performed a comparative study of the flow of the nanofluid flows comprising CNTs of both types with two base liquids considering the Darcy-Forchheimer and homogeneous-heterogeneous reactions amalgamated with second-order slip at the surface of an extended sheet. The problem is addressed numerically, and outcomes are presented in the forms of graphs and tables. It is comprehended that the effect of the aqueous-based single-wall CNTs fluid performed better than multi-wall CNTs fluid as far as fluid concentration is concerned.

In the study of oceanic sciences and atmospheric, fluid stratification is a phenomenon of liquid layering owing to differences in densities, temperature, or composition. This phenomenon is common in chemical industrial processes, environmental science, meteorology, atmosphere, oceanography, and bodies of water. The dynamics of stratification are also important for solar engineering because stratification may predict the chance of attaining higher energy capability. A strong propensity of the researchers/scientists toward the stratification phenomenon has been observed in the recent past. Hamid *et al.* [6] discussed the doubly stratified effect of Williamson nanofluids with mixed convection and thermal radiation. They employed the Runge-Kutta Fehlberg method to solve the model. They also reported that for declining values of mass transfer rate, the Brownian motion parameter increases. The double stratification with MHD flow of nanoliquid and slip conditions is investigated by Hayat *et al.* [7]. They employed HAM to attain the series solution of the system. They also discussed that the concentration profile increases and temperature distribution reduces for higher estimations of the thermophoretic and thermal stratification parameters respec-

tively. Ramzan *et al.* [8] discovered the influences of Cattaneo-Christov heat flux with stratified media in Darcy Forchheimer nanofluid flow comprising carbon nanotubes and homogeneous-heterogeneous reactions. The effect of nanofluid flow containing CNTs with an upper permeable wall in a rotating channel by using ethylene-glycol as a base fluid is discussed by Ramzan *et al.* [9]. It is witnessed that fluid temperature is on the decline for the thermal stratification parameter.

The aforementioned literature demonstrates that a lot of effort has been observed by the researchers to discuss the effect of single-wall CNTs on nanofluid flow. However, less attention is paid to the effect of Cattaneo-Christov heat flux and thermal radiation with single-wall CNTs immersed in nanofluid flow. Nonetheless, no work has been done so far on single-wall CNTs with heat transfer and MHD nanofluid flow with mixed convection over an inclined stretching sheet. The partial slip at the boundary wall is also taken into consideration. The effect of heat generation absorption and stratification boundary conditions is also considered. Irreversibility analysis is also a part of the present study. Utilizing the bvp4c MATLAB software function, the envisaged model is numerically addressed. The outcomes of the mathematical model are reported through diagrams and tables.

2. Mathematical Formulation

Let us assume a two-dimensional, mixed convection, electrically conducting nanofluid flow along the permeable stretching surface with a velocity $U_w(x) = cx$, leaning at an angle of $(\alpha = 45^\circ)$ with the horizontal axis (**Figure 1**). The nanofluid is comprised of single-wall carbon nanotubes and ethylene glycol mixture. The heat transfer behavior has been examined by considering the uniform electric and magnetic fields with the stratified medium.

The boundary layer governing equations are represented as:

$$u_x + v_y = 0, \quad (1)$$

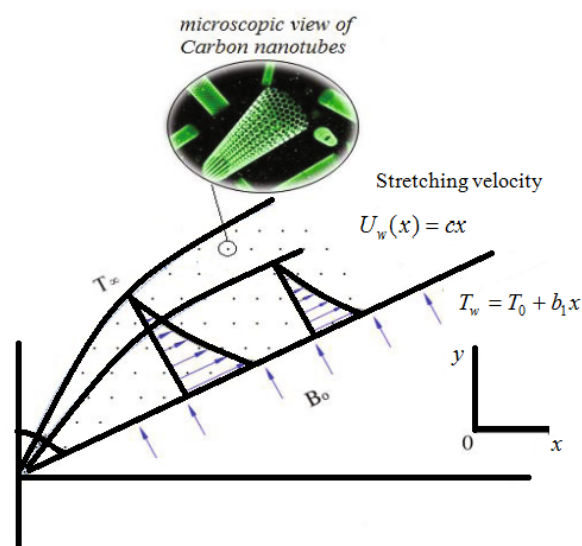


Figure 1. Flow geometry of the assumed model.

$$uu_x + vv_y = v_s u_{yy} + g \frac{(\beta\rho)_s}{\rho_s} (T - T_\infty) \cos \alpha + \frac{\sigma}{\rho_s} (E_0 B_0 - B_0^2 u). \tag{2}$$

Mathematically, the pattern of heat transfer can be described as follows:

$$\rho c_p (uT_x + vT_y) = -\nabla \cdot \mathbf{q}. \tag{3}$$

The Cattaneo-Christov heat flux expression is given as under:

$$\mathbf{q} + \lambda(\mathbf{q}_t - \mathbf{q} \cdot \nabla \mathbf{V} + \mathbf{V} \cdot \nabla \mathbf{q} + (\nabla \cdot \mathbf{V})\mathbf{q}) = -K \nabla T, \tag{4}$$

For $\lambda = 0$, Equation (4) changes the Fourier's law. Equation (4) for incompressibility conditions yields:

$$\mathbf{q} - \lambda(\mathbf{q} \cdot \nabla \mathbf{V} - \mathbf{V} \cdot \nabla \mathbf{q}) = -K \nabla T. \tag{5}$$

Removing \mathbf{q} from Equations (3) and (5), we obtain:

$$\begin{aligned} uT_x + vT_y = & \frac{\kappa_s}{(\rho c_p)_s} T_{yy} - \lambda_2 (u^2 T_{xx} + v^2 T_{yy} + 2uv T_{xy} + (uu_x + vv_y) T_x \\ & + ((uv_x + vv_y) T_y) + \frac{1}{(\rho c_p)_s} \frac{16\sigma^* T_\infty^3}{3k^* (\rho c_p)_s} T_{yy} + \frac{Q_0(T - T_\infty)}{(\rho c_p)_s} + \frac{\sigma(uB_0 - E_0)^2}{(\rho c_p)_s}, \end{aligned} \tag{6}$$

The boundary constraints are:

$$\begin{aligned} u = U_w + U_s, \quad v = V_w, \quad T = T_w = T_0 + b_1 x \quad \text{at } y = 0, \quad U_s = l u_y \Big|_{y=0}, \\ u \rightarrow 0, \quad T = T_\infty = T_0 + b_2 x \quad \text{as } y \rightarrow \infty \end{aligned} \tag{7}$$

To transmute the envisioned model to the system of ODEs, we assume the subsequent transformations:

$$u = cxf'(\eta), \quad v = -\sqrt{cv_f} f(\eta), \quad \theta(\eta) = \frac{T - T_\infty}{T_w - T_\infty} \quad \text{at } \eta = \sqrt{\frac{c}{v_f}} y \tag{8}$$

The above transformation converts the Equations (2), (6), and (7) as given as:

$$\begin{aligned} & \frac{(1-\phi)^{-2.5}}{\left(1-\phi + \frac{\rho_{cnt}}{\rho_f} \phi\right)} f''' + ff'' - f'^2 + \frac{\left(1-\phi + \frac{(\beta\rho)_{cnt}}{(\beta\rho)_f} \phi\right) \lambda \cos \alpha}{\left(1-\phi + \frac{\rho_{cnt}}{\rho_f} \phi\right)} \theta \\ & + \frac{1}{\left(1-\phi + \frac{\rho_{cnt}}{\rho_f} \phi\right)} (M^2 E - M^2 f') = 0 \\ & \frac{(1-\phi)^{-2.5} \frac{\kappa_s}{\kappa_f}}{\left(1-\phi + \frac{\rho_{cnt}}{\rho_f} \phi\right)} \frac{1}{Pr} \theta'' + fP - 2\theta f' + f\theta' - \gamma_1 (4f'^2 \theta - 3ff'\theta' + f^2 \theta'') \\ & + \frac{Ec}{\left(1-\phi + \frac{\rho_{cnt}}{\rho_f} \phi\right)} (f'')^2 + \frac{Q}{\left(1-\phi + \frac{\rho_{cnt}}{\rho_f} \phi\right)} \theta + \left(1-\phi + \frac{\rho_{cnt}}{\rho_f} \phi\right) (f'^2 + E^2 - 2Ef') \\ & + \frac{4}{3\left(1-\phi + \frac{\rho_{cnt}}{\rho_f} \phi\right)} Rd\theta'' = 0, \end{aligned} \tag{10}$$

$$f(0) = S, f'(0) = 1 + \zeta f''(0), \theta(0) = 1 - P, \\ f'(\infty) = 0, \theta(\infty) = 0, \tag{11}$$

where

$$P = \frac{b_2}{b_1}, \lambda = \frac{g\beta_f(T_w - T_\infty)}{cU_w}, Pr = \frac{\nu_f}{\alpha_f^*}, Ec = \frac{U_w^2}{C_p(T_w - T_\infty)}, M = \frac{\sigma B_0^2}{C_p}, \\ Rd = \frac{4\sigma^* T_\infty^3}{kk^*}, Q = \frac{Q_0}{(\rho C_p)c}, E = \frac{E_0}{u_w B_0}, \zeta = l \sqrt{\frac{c}{\nu_f}}, S = \frac{-v_w}{\sqrt{c\nu_f}}, \gamma_1 = \lambda_2 c. \tag{12}$$

The drag force coefficient C_f is presented as:

With

$$\tau_w = \mu_{nf}(u_y)_{y=0}. \tag{13}$$

Dimensionless form of drag force coefficient is given as:

$$C_f \sqrt{Re_x} = \frac{f''(\eta)}{(1-\phi)^{2.5}}, \tag{14}$$

where $Re_x = xU_w / \nu_f$ is the local Reynolds number.

Table 1 and **Table 2** represent the thermo-physical values of the nanofluid being considered.

3. Graphical Discussion

In this section, the outcomes are depicted in the form of graphs for velocity and temperature profiles versus discrete values of the arising flow parameters. The

Table 1. Thermophysical values of the base liquid and single-wall CNTs.

Physical properties	Ethylene glycol	SWCNT
$\rho(kgm^{-3})$	1115	2600
$c_p \left(\frac{kg.K}{J}\right)^{-1}$	2430	425
$K \left(\frac{mK}{W}\right)^{-1}$	0.253	6600

Table 2. Thermophysical attributes of nanoliquid.

Density	$\rho_s = (1-\phi)\rho_f + \phi\rho_{cnt}$
Heat capacity	$(\rho c_p)_s = (1-\phi)(\rho c_p)_f + \phi(\rho c_p)_{cnt}$
Variable viscosity	$\mu_s = \mu_f(1-\phi)^{-2.5}$
Thermal conductivity	$\frac{\kappa_s}{\kappa_f} = \frac{2\phi \frac{\kappa_{cnt}}{\kappa_{cnt} - \kappa_f} \ln\left(\frac{\kappa_{cnt} + \kappa_f}{2\kappa_f}\right) + 1 - \phi}{2\phi \frac{\kappa_f}{\kappa_{cnt} - \kappa_f} \ln\left(\frac{\kappa_{cnt} + \kappa_f}{2\kappa_f}\right) + 1 - \phi}$
Thermal expansion	$(\beta\rho)_s = (1-\phi)(\beta\rho)_f + \phi(\beta\rho)_{cnt}$

values of these parameters are fixed as $Pr = 204$, $Ec = 0.3$, $E = 0.2$, $M = 0.2$, $S = 1.0$, $Rd = 0.6$, $Q = 0.2$, $\gamma_1 = 0.5$, $\lambda = 0.5$, $P = 0.1$ unless otherwise stated.

The impact of the magnetic parameter M on the fluid velocity profile f' is displayed in **Figure 2**. It is seen that fluid velocity is declined for the high values of M . This is because of the strong Lorentz force that hinders the fluid flow and a drop in the velocity of the liquid is observed. **Figure 3** depicts the behavior of the thermal convection parameter (λ) versus the fluid velocity profile. It is noted

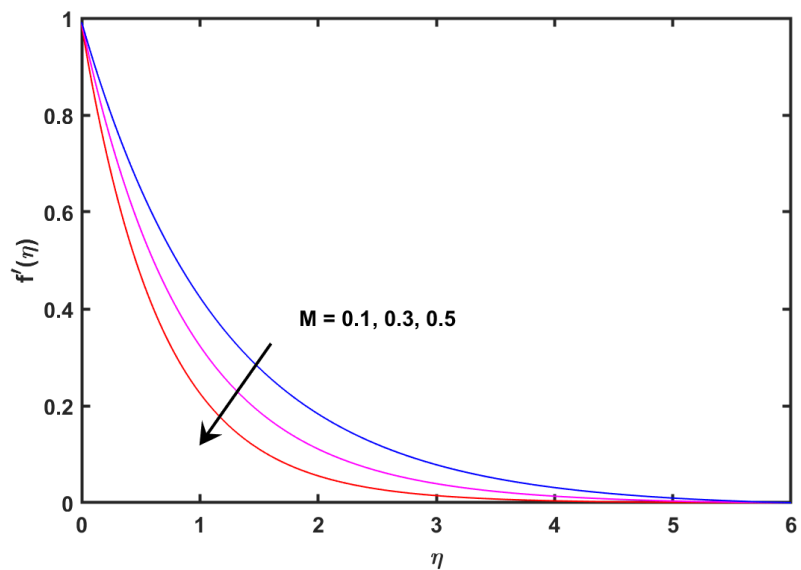


Figure 2. Fluid velocity profile f' versus changes in magnetic parameter M .

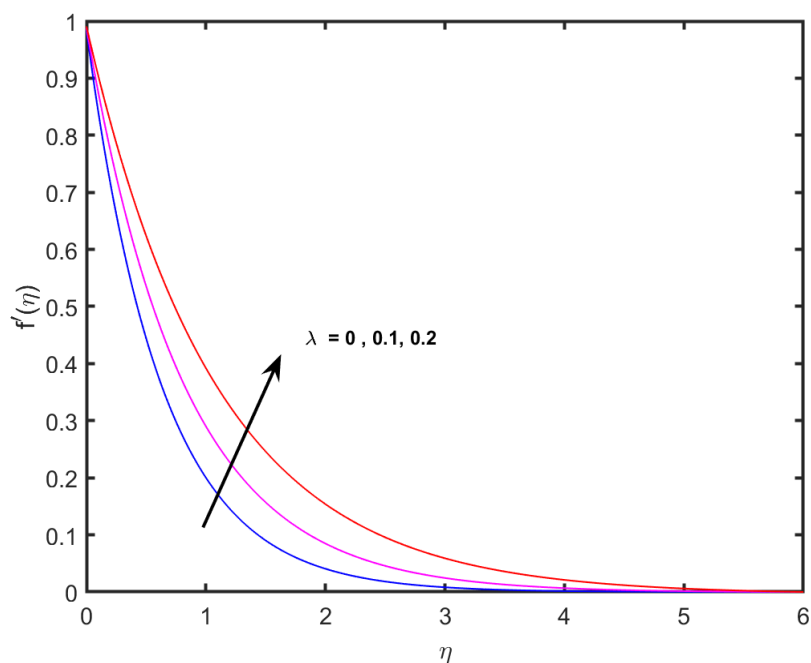


Figure 3. Fluid velocity profile f' versus changes in thermal convection parameter λ .

that the fluid velocity is augmented for varied estimates of the (λ). A surge in the Nusselt number means the high heat transfer rate leads to high thermal convection. This only occurs when there is an increase in the fluid velocity is noted. The association of the suction parameter (S) with the fluid velocity is illustrated in **Figure 4**. A decline in the fluid velocity is noticed here. The fluid momentum is on the decline when there is a strong effect of the suction. Eventually, the fluid velocity decreases. **Figure 5** is displayed to describe the correlation between the thermal relaxation parameter (γ_1) and the fluid temperature profile. Here, high

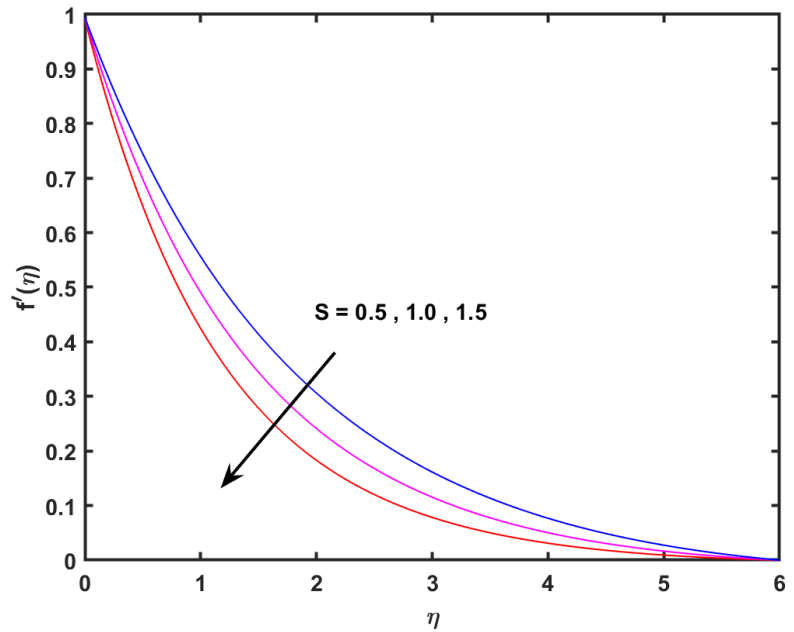


Figure 4. Fluid velocity profile f' versus changes in suction parameter S .

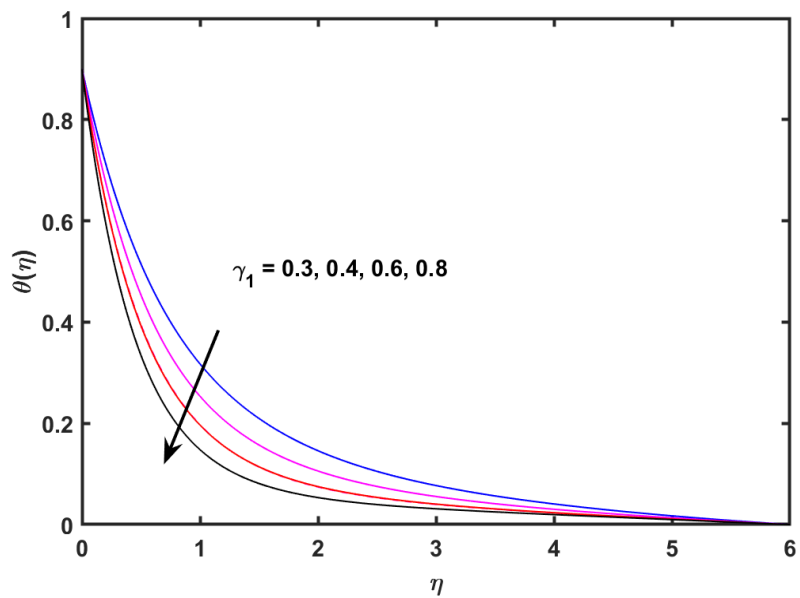


Figure 5. Fluid temperature profile θ versus changes in thermal relaxation parameter γ_1 .

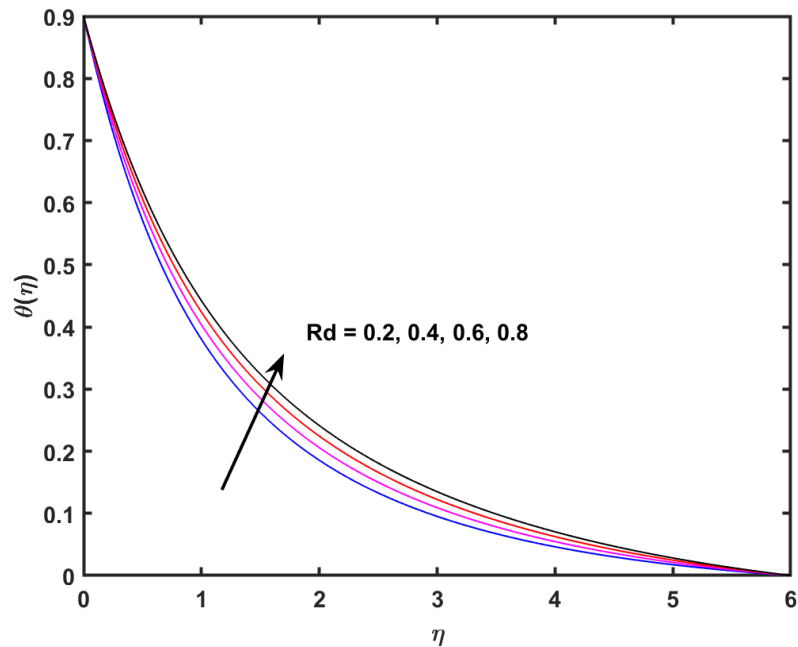


Figure 6. Fluid temperature profile θ versus changes in radiation parameter Rd .

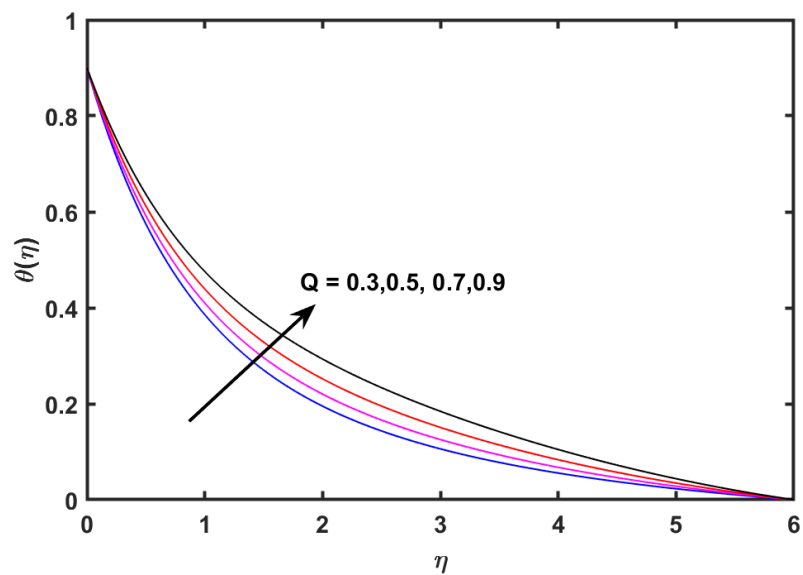


Figure 7. Fluid temperature profile θ versus changes in heat absorption/generation parameter Q .

estimates of (γ_1) result in a fall in the fluid temperature. This is due to the increased duration required for fluid particles to convey heat to adjacent particles. The impact of the radiation parameter (Rd) on the temperature profile is depicted in **Figure 6**. A surge in the fluid temperature profile is witnessed for (Rd). Higher values of (Rd) mean more heat is radiated and is being transferred to the fluid leading to a significant addition to fluid temperature. **Figure 7** is demonstrated to perceive the influence of the heat absorption/generation parameter (Q) on the fluid temperature profile. The last thermal equilibrium of the system

is disrupted owing to a rise in the values of (Q) causing the fluid temperature to adjust with the latest changes leading to an increment in the fluid temperature profile. The impact of the stratification parameter (P) on the thermal profile is given in **Figure 8**. The thermal profile falls when we strengthen the estimation of (P). The layers of the fluid behave becomes insulating when there is a strong effect of the thermal stratification leading to insulation effect between the layers of the fluid and the surroundings. So, less heat is transmuted to the liquid leading to a drop in the fluid temperature.

The graph for Eckert number Ec and nanoparticle concentration ϕ versus Skin friction coefficient is depicted in **Figure 9**. It is perceived that the skin friction coefficient shows an opposite trend for Ec and ϕ . **Figure 10** is drawn to see the impact of the thermal convection parameter λ and nanoparticle concentration ϕ on the Skin friction coefficient. Similar behavior is witnessed here for λ and ϕ .

4. Irreversibility Analysis

The volumetric entropy generation N_s is presented as:

$$S_{GEN}''' = \frac{\kappa_s}{T_\infty^2} T_Y'^2 + \frac{\mu_s}{T_\infty} u_Y'^2 + \frac{\sigma B_0^2}{T_\infty} u^2. \tag{15}$$

The N_s in non-dimensional form is:

$$N_s = \frac{S_{GEN}'''}{S_0'''} = Re \left(\frac{\kappa_s}{\kappa_f} (\theta'(\eta))^2 + (1-\phi)^{-2.5} \frac{Br}{\Omega} (f^2(\eta) + M^2 f'^2(\eta)) \right), \tag{16}$$

where

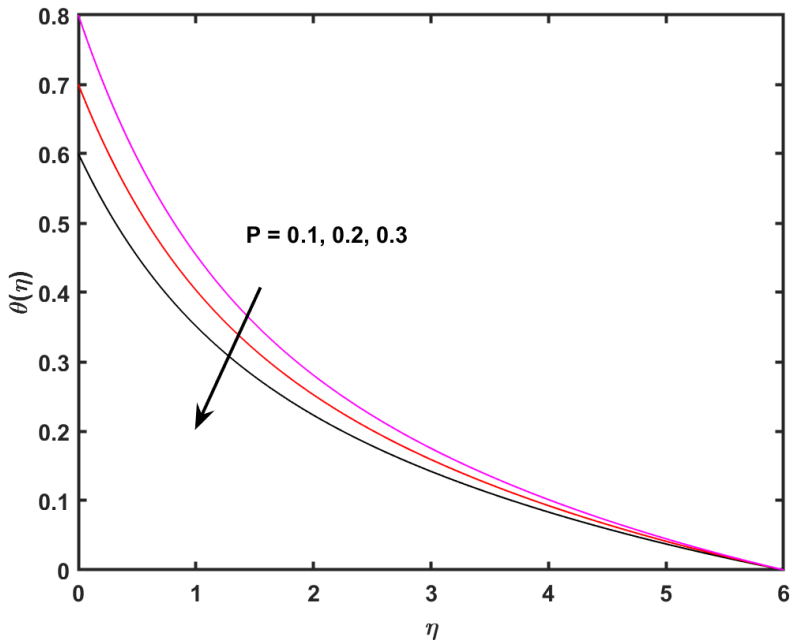


Figure 8. Fluid temperature profile θ versus changes in thermal stratification parameter P .

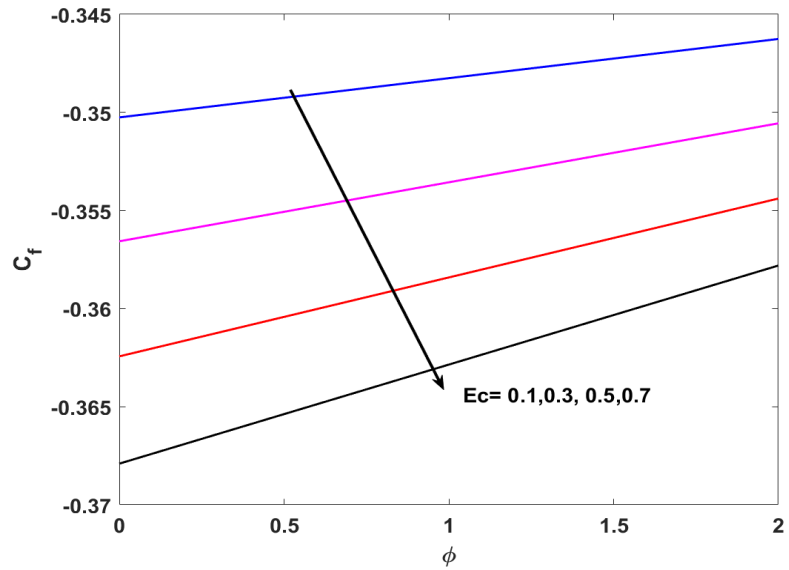


Figure 9. Surface drag coefficient C_f versus changes in Eckert number Ec and nanoparticle volume fraction ϕ .

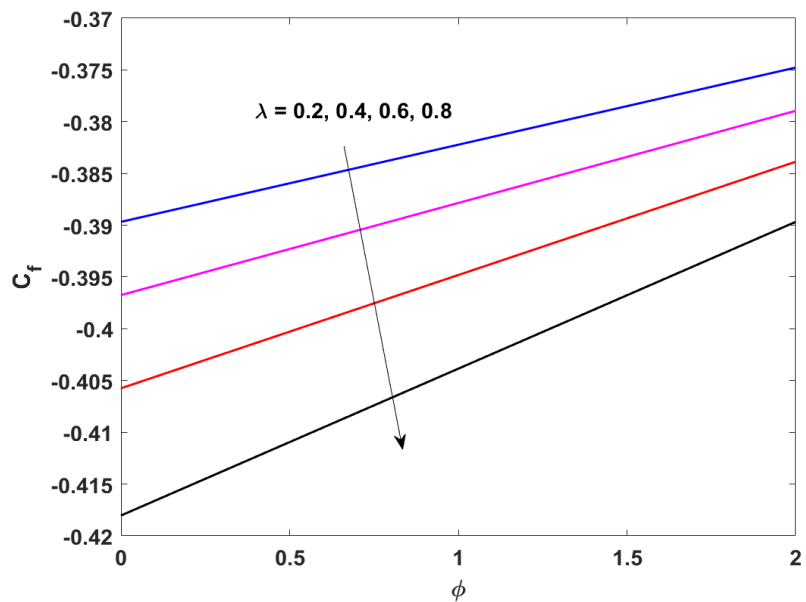


Figure 10. Surface drag coefficient C_f versus changes in thermal convection parameter λ and nanoparticle volume fraction ϕ .

$$S_0^m = \frac{k_f \Omega \nabla T}{v_f T_\infty}, \quad Re = \frac{u_w}{v_f}, \quad Br = \frac{\mu_f u_w^2}{k_f (T_w - T_\infty)}, \quad \Omega = \frac{T_w - T_\infty}{T_\infty} \quad (17)$$

The Bejan number (Be) is stated as:

$$Be = \frac{\frac{\kappa_s}{T_\infty} T_y^2}{\frac{\mu_s}{T_\infty} u_y^2 + \frac{\sigma B_0^2}{T_\infty} u^2} \quad (18)$$

The Be in non-dimensional form is given by:

$$Be = \frac{(1 - \varphi)^{2.5} \frac{\kappa_s}{T_\infty^2} Re\theta^2}{Re\left(\frac{Br}{\Omega} f'^2 + \frac{Br}{\Omega} M^2 f'^2\right)} \tag{19}$$

Figure 11 and **Figure 12** show important features of the thermal convection parameter λ and Eckert number Ec versus entropy generation profile N_s . In these figures, less entropy generation is observed for both parameters.

5. Final Comments

In our current investigation, we have examined the flow of single-wall carbon

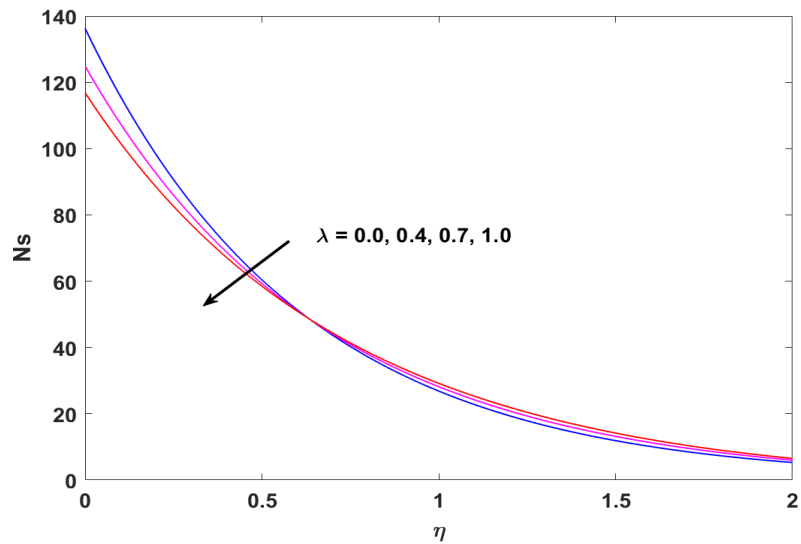


Figure 11. Entropy generation profile N_s versus changes in thermal convection parameter λ .

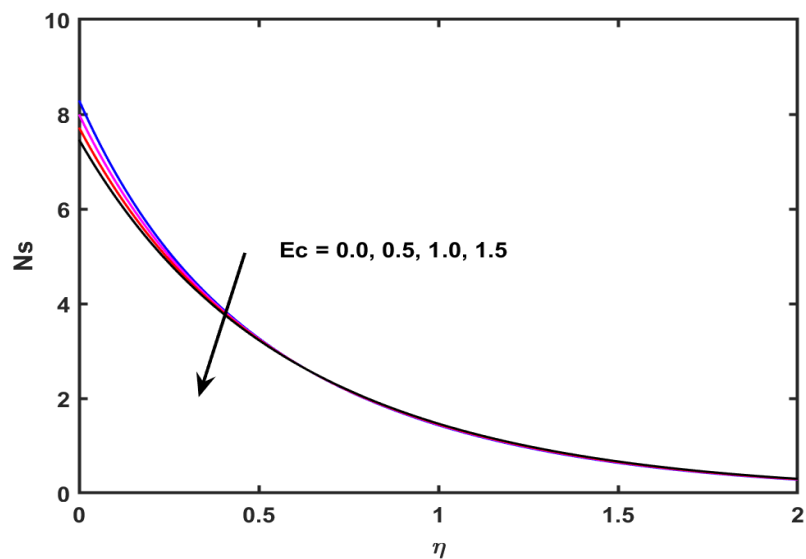


Figure 12. Entropy generation profile N_s versus changes in Eckert number Ec .

nanotubes (CNTs) dispersed in ethylene glycol nanofluid on an inclined extended surface under the influence of mixed convection. Our analysis considers heat transfer in the presence of a heat source/sink, as well as thermal stratification effects and Cattaneo-Christov heat flux. The problem is tackled using numerical methods. The principal findings of our proposed model are outlined below:

- The velocity profile shows an opposing trend for thermal convection and suction parameters.
- The fluid velocity is on the decline for a strong magnetic field.
- The fluid temperature is on the decline for the thermal stratification and thermal relaxation parameters.
- For heat absorption/generation and thermal radiation parameters, the fluid temperature upsurges.
- The skin friction coefficient depicts conflicting behavior for the Eckert number and nanoparticle volume concentration.
- The entropy generation profile is on the decline for the Eckert number and thermal convection parameter.

Conflicts of Interest

The authors declare no conflicts of interest regarding the publication of this paper.

References

- [1] Wang, J., Zhu, J., Zhang, X. and Chen, Y. (2013) Heat Transfer and Pressure Drop of Nanofluids Containing Carbon Nanotubes in Laminar Flows. *Experimental Thermal and Fluid Science*, **44**, 716-721. <https://doi.org/10.1016/j.exptthermflusci.2012.09.013>
- [2] Iqbal, Z., Azhar, E. and Maraj, E.N. (2017) Transport Phenomena of Carbon Nanotubes and Bioconvection Nanoparticles on Stagnation Point Flow in Presence of the Induced Magnetic Field. *Physica E: Low-Dimensional Systems and Nanostructures*, **91**, 128-135. <https://doi.org/10.1016/j.physe.2017.04.022>
- [3] Alharbi, K.A.M., Ramzan, M., Shahmir, N., Ghazwani, H.A.S., Elmasry, Y., Eldin, S.M. and Bilal, M. (2023) Comparative Appraisal of Mono and Hybrid Nanofluid Flows Comprising Carbon Nanotubes over a Three-Dimensional Surface Impacted by Cattaneo-Christov Heat Flux. *Scientific Reports*, **13**, Article No. 7964. <https://doi.org/10.1038/s41598-023-34686-8>
- [4] Gul, H., Ramzan, M., Saleel, C.A., Kadry, S. and Saeed, A.M. (2023) Heat Transfer Analysis of a Moving Wedge with Impact of Nano-Layer on Nanofluid Flows Comprising Magnetized Carbon Nanomaterials. *Numerical Heat Transfer, Part A: Applications*, 1-14. <https://doi.org/10.1080/10407782.2023.2240498>
- [5] Bashir, S., Almanjahie, I.M., Ramzan, M., Cheema, A.N., Akhtar, M. and Alshahrani, F. (2024) Impact of Induced Magnetic Field on Darcy-Forchheimer Nanofluid Flows Comprising Carbon Nanotubes with Homogeneous-Heterogeneous Reactions. *Heliyon*, **10**, E24718. <https://doi.org/10.1016/j.heliyon.2024.e24718>
- [6] Hamid, A., Alghamdi, M., Khan, M. and Alshomrani, A.S. (2019) An Investigation of Thermal and Solutal Stratification Effects on Mixed Convection Flow and Heat Transfer of Williamson Nanofluid. *Journal of Molecular Liquids*, **284**, 307-315.

<https://doi.org/10.1016/j.molliq.2019.03.181>

- [7] Hayat, T., Nasseem, A., Khan, M.I., Farooq, M. and Al-Saedi, A. (2018) Magnetohydrodynamic (MHD) Flow of Nanofluid with Double Stratification and Slip Conditions. *Physics and Chemistry of Liquids*, **56**, 189-208.
<https://doi.org/10.1080/00319104.2017.1317778>
- [8] Ramzan, M. and Shaheen, N. (2019) Thermally Stratified Darcy Forchheimer Nanofluid Flow Comprising Carbon Nanotubes with Effects of Cattaneo-Christov Heat Flux and Homogeneous-Heterogeneous Reactions. *Physica Scripta*, **95**, Article ID: 015701. <https://doi.org/10.1088/1402-4896/ab3d06>
- [9] Ramzan, M., Gul, H. and Kadry, S. (2019) Onset of Cattaneo-Christov Heat Flux and Thermal Stratification in Ethylene-Glycol Based Nanofluid Flow Containing Carbon Nanotubes in a Rotating Frame. *IEEE Access*, **7**, 146190-146197.
<https://doi.org/10.1109/ACCESS.2019.2945594>

Nomenclature

A, b_1, b_2, c	Dimensional constant
E	Electrical parameter
λ	Thermal convective parameter
κ_s	Thermal conductivity of nanofluid
S	Suction parameter
Pr	Prandtl number
P	Thermal stratification parameters
μ_s	Viscosity of nanofluid
T	Liquid temperature
β_s	Coefficient of thermal expansion
φ	Nanoparticle volumetric
E_0	Electric field parameter
M	Magnetic field parameter
S_0''	Characteristic entropy generation
μ_f	Dynamic viscosity of a liquid
U_w, V_w	Stretching linear velocity
Be	Bejan number
β	Thermal expansion coefficient
Rd	Radiation parameter
C_f	Drag force
V_0	Uniform suction
$(\rho c)_s$	Ratio of heat capacity
Ec	Eckert number
Re_x	Reynolds number
T_w	Temperature on wall
\mathbf{T}	Viscous stress tensor
ρ_s	Density of nanofluid
$(c_p)_s$	Specific heat capacity of nanofluid
f	Base fluid
(u, v, w)	Components of velocities
γ_1	Thermal relaxation parameter
κ	Thermal conductivity
ν_f	Kinematic viscosity
N_s	Entropy generation rate
Q_0	Heat generation parameter
Br	Brinkman number